ACS OMEGA

Open Access

http://pubs.acs.org/journal/acsodf

Article

Cyan Hydrogen Process: A New Route for Simultaneous Hydrogen Production and Carbon Valorization

Alessandra Di Nardo, Maria Portarapillo, Danilo Russo, Giuseppina Luciani, Gianluca Landi, Giovanna Ruoppolo, Alessandro Pezzella, and Almerinda Di Benedetto*

Cite This: *ACS Omega* 2024, 9, 7793−7805

Read Online

ACCESS | Metrics & More | Article Recommendations | Supporting Information

ABSTRACT: Hydrogen is expected to largely contribute to the near-future circular economy. Today, most hydrogen is still produced from fossil fuels or renewable pathways with low efficiency and high cost. Herein, a proof of concept for a novel hydrogen production process is proposed, here named cyan hydrogen, inspired by a combination of the green and blue processes, due to the key role played by water and the low carbon content in the gas phase, respectively. The developed novel process, recently patented and demonstrated at the lab scale, is based on successive steps in which ethanol (5.0 mL) and water (10.0 mL) are alternately fed, with a fixed initial amount of sodium metaborate (2.0 g), in a batch reactor at 300 °C. Preliminary results showed the simultaneous production of a 95% v/v hydrogen stream, a polymeric byproduct with a repetitive carbon pattern $-CH_2-CH_2-$, and a liquid phase rich in oxygenated chemicals at temperatures lower than conventional hydrogen production processes.

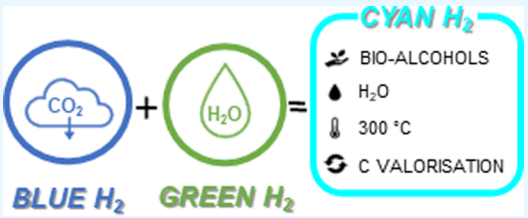

INTRODUCTION

The chemical industry has a key role in the development of a circular sustainable economy, integrating the needs of the society and environment.[1] According to the European Union directives and the Paris Agreement, hydrogen and gas infrastructures will play a fundamental role in the transition to a climate neutral economy by 2050.[2] Nevertheless, on a global scale, the use of renewable materials and energy is problematic, with oil, natural gas, and coal still covering most of the world energy consumption.[3]

Hydrogen is one of the main building blocks of the bulk and fine chemical industries and a promising energy carrier. However, most hydrogen is currently produced from fossil fuels, via hydrocarbon reforming or pyrolysis processes.[4] Routes from renewable sources include biological and thermochemical treatment of biomass,[5] water splitting,[6] and water plasmolysis.[7]

In the present public debate over hydrogen economy, different color codes have been used to identify hydrogen, depending on the adopted production process and, more specifically, on the employed raw materials and energy source (solar, electricity, hydro, nuclear power, or gas). The colors include green, blue, gray, pink, and yellow.[8] Several reviews[9,10] report technological and economic comparisons of different hydrogen colors. In Figure 1, a scheme of the main differences between different H_2 colors is shown.

As mentioned above, the dominant technologies for hydrogen production are methane steam reforming, which accounts for 59% of the total global hydrogen production, and coal gasification, accounting for about 20% globally, resulting in 830 Mt/year CO_2 emissions.[11,12] The hydrogen produced through these technologies is referred to as gray and black hydrogen, respectively. Similarly, blue hydrogen still refers to H_2 from fossil fuels but in combination with CO_2 capture technologies. Overall, 90% capture can be achieved in an integrated steam methane reforming system with a relatively low energy penalty (5−14%).[11,13] Soon, a transition from gray to blue hydrogen is expected. Blue hydrogen is a rather mature technology, already implemented in some transport systems.[14] However, it starts from fossil fuels and operates at relatively high temperatures, and the CO_2 capture, mainly based on the CO_2 adsorption, is not easy to realize and manage. Furthermore, due to additional costs for carbon capture and storage, the costs of gray hydrogen range from 0.8 to 2.6 USD/kg H_2, depending on the country.[15] Up to date, the most adopted alternative H_2 production process is based on water splitting by electrolysis. The so-called green hydrogen is produced by using electrical energy from renewable energy sources, such as wind or solar, with no carbonaceous byproducts.[16] However, the estimated production cost and energy efficiency for electrolysis are 10.3 USD/kg and 52%, respectively. Electrolysis, an energy-intensive process for hydrogen production, is still confronting challenges from a

Received: September 21, 2023
Revised: October 30, 2023
Accepted: November 6, 2023
Published: February 8, 2024

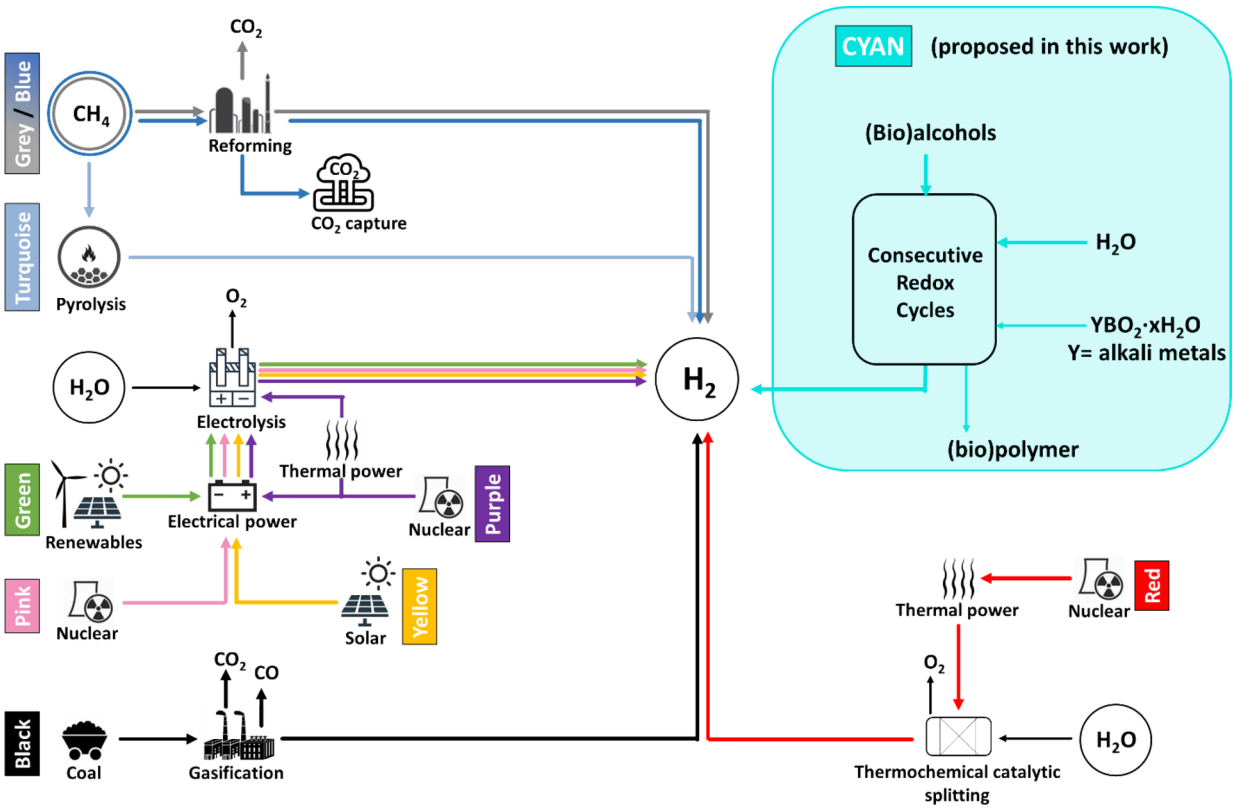

Figure 1. Overview of the most common hydrogen production processes and their color code.

cost perspective.[7] Research in this field mainly focuses on the electrolytic cell devices and the electrocatalysts.[17] Similarly to green hydrogen, pink and yellow hydrogens are both produced through water electrolysis but using exclusively nuclear or solar energy, respectively.[8] Thermochemical electrolysis of water from nuclear energy results in purple hydrogen, and high-temperature catalytic water splitting using nuclear energy is classified as red hydrogen.[14] Turquoise hydrogen, like gray and blue, uses methane as a feedstock. However, in this case, methane pyrolysis results in hydrogen with carbon removed in a solid form rather than CO_2.[18] In Table 1 are reported feedstock, products, and operating conditions of commercial hydrogen production processes, labeled by their color codes.

To enable the use of renewable hydrogen at different scales, intensive technology development is required to increase the efficiency of renewable existing processes and reduce their cost as well as to develop innovative processes. In this scenario, the here proposed hydrogen production process, labeled "cyan hydrogen", based on patent WO 2023/105545 A1,[19] is inspired by a combination of the green and blue processes due to the key role played by water and the low carbon content in the produced gas phase, respectively (Figure 1).

The proposed process consists of consecutive redox cycles carried out in batch conditions and allows the production of a high-purity H_2 stream starting from bioalcohols and/or biodiols, water, and oxidized byproducts of hydrides commonly used for hydrogen storage such as alkali metal salts of metaborate ($YBO_2{\cdot}xH_2O$, with a Y alkali metal and an x water content). Thus, hydrogen generation can take place simultaneously with a solid polymer-borate mixture and with oxygenated chemical production in the liquid phase, under conditions (300 °C) milder than those normally adopted for natural gas steam reforming (800 °C).

Table 1. Feedstock, Products, and Operating Temperatures of the Main Hydrogen Production Processes Are Classified According to Color Codes

HYDROGEN COLOR	FEEDSTOCK	PRODUCTS	OPERATING CONDITIONS
BLACK	Coal	H_2, CO, CO_2, CH_4	800 - 1600 °C
GREY	Natural gas	H_2, CO, CO_2	700 - 1000 °C
BLUE	Natural gas	H_2, $CO_{2(captured)}$, CO	700 - 1000 °C
GREEN	Water	H_2, O_2	100 - 900 °C (based on the used technology)
TURQUOISE	Natural gas	H_2, $C_{(s)}$	1100 - 1200 °C
CYAN (proposed in this work)	Bio-alcohols	H_2, polymer, organic liquid	300 °C

In the present work, we report a proof of concept, showing the preliminary results of the developed cyan hydrogen production process carried out by using a target molecule, i.e., (bio)ethanol, and sodium metaborate ($NaBO_2{\cdot}4H_2O$).

Sodium metaborate is a readily available and relatively cheap oxide (1−15 USD/kg depending on purity grade) that can be obtained from the refinery of natural mineral tincalconite or from the reaction between borax and caustic soda[20] with a wide range of applications, i.e., production of sodium perborate, stabilizer in textile processing, adhesives, corrosion inhibitor, detergent, and cleaners.[21] It is also a byproduct of the

https://doi.org/10.1021/acsomega.3c07277
ACS Omega 2024, 9, 7793−7805

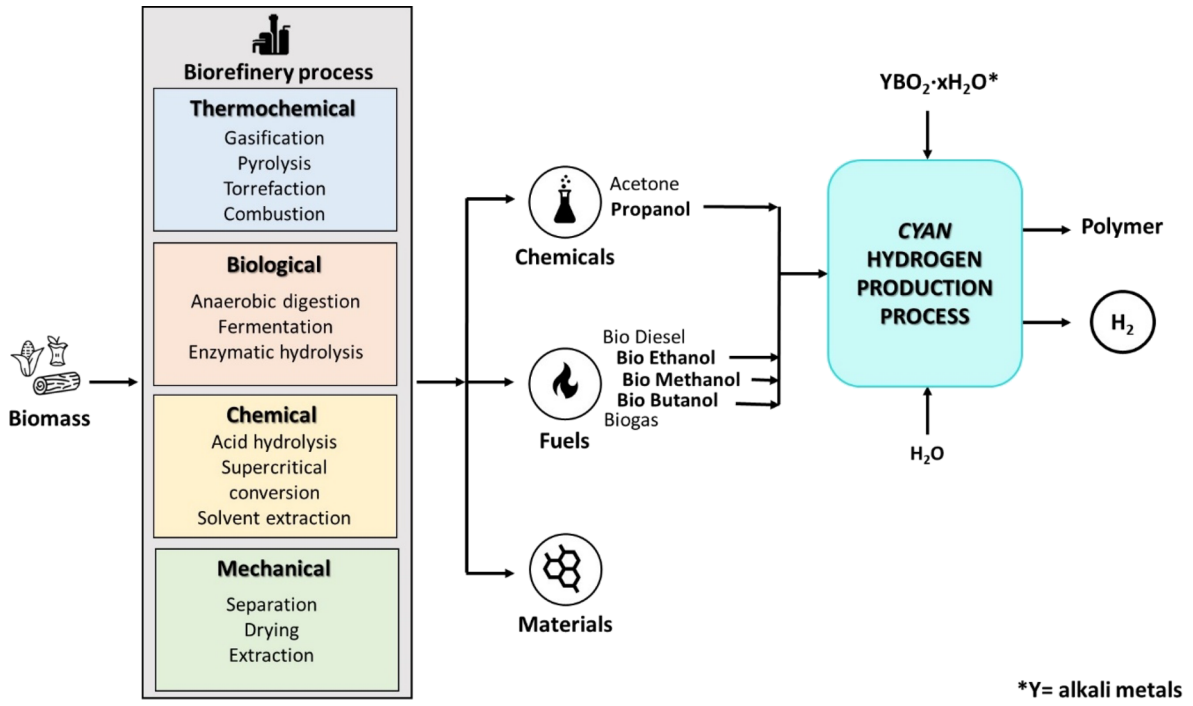

Figure 2. Schematic representation of biorefinery pathways and integration of produced bioalcohols into cyan hydrogen production.

hydrolysis reaction of sodium borohydride ($NaBH_4$), which is commonly investigated for hydrogen storage.[22] In aqueous solution, $NaBH_4$ is capable of undergoing a catalyzed hydrolysis reaction, releasing 90% of the stoichiometric hydrogen and producing sodium metaborate $NaBO_2$ according to the following equation (eq 1):[23]

$$NaBH_4 + 2H_2O \rightarrow NaBO_2 + 4H_2 \quad (1)$$

The bottleneck for the wide adoption of $NaBH_4$ for hydrogen storage is represented by the difficult regeneration of $NaBH_4$ from $NaBO_2$, consisting of a tedious multistep process, which is inefficient and expensive and has a significant environmental impact.[24] Alternatively, it has been proposed to convert $NaBO_2$ into hydride using a reducing agent such as coke or CH_4. However, a study has shown that the reaction is only favored at $T > 1000$ °C.[25]

In order to produce clean and emission-free hydrogen, the raw materials must also be obtained accordingly. In biorefineries, bioalcohols can be produced from a variety of biomasses, including first- and second-generation feedstocks, through different pathways, as shown in Figure 2. The most frequent production routes for bioethanol and biobutanol include fermentation, iso-propanol can be made by reducing acetone produced by acetone-butanol-ethanol (ABE) fermentation, and biomethanol is commonly produced via the thermochemical pathway.[26,27] In particular, bioethanol is generally produced by fermenting the sugar and starch components of plant byproducts such as sugar cane, maize, and wheat.[28] In addition to being used as an additive/alternative to petrol, bioethanol can be regarded as a feedstock for various processes, predominantly hydrogen or ethylene production.[29]

In this framework, the cyan hydrogen process shown in this work starts from bioethanol in the presence of water and sodium metaborate (Figure 3), following a consecutive redox cycle scheme. A preliminary physicochemical investigation was

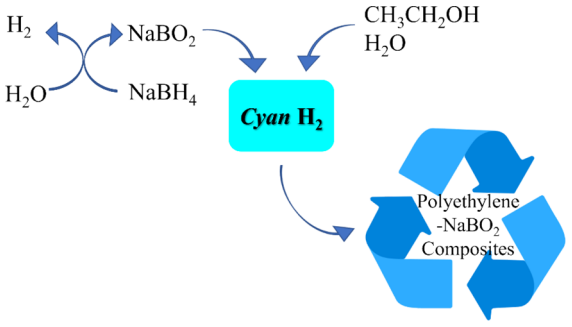

Figure 3. Scheme of the reagents, sodium metaborate, ethanol, and water, and the products, a polyethylene-borate mixture, of the cyan hydrogen production process.

carried out on the solid, liquid, and gas phases recovered during each stage of this multistep process. Preliminary results show the formation of an organic polymeric solid phase and liquid oxygenated products. A detailed and thorough chemical characterization of such phases is beyond the scope of the present work and will be further addressed by future research.

EXPERIMENTAL SECTION

Materials. Sodium metaborate tetrahydrate (CAS: 10555-76-7, Sigma-Aldrich, ≥99%), ethanol (CAS: 64-17-5, Sigma-Aldrich, ≥99.0%), and Milli-Q water were used in all experimental runs. Nitrogen (6.0 grade, supplied by SOL Srl in high-pressure cylinders) was used for inerting procedures and to pressurize the reactor.

α-Cyano-4-hydroxycinnamic acid (CHCA, 98% purity), HPLC-grade ethanol, cyclohexane, acetonitrile, trifluoroacetic acid (TFA), and water used for MALDI-TOF analysis were purchased from Sigma-Aldrich and used as received.

Experimental Setup. Experimental tests were carried out in a batch reactor (V = 450 mL, model 4567, Parr Instrument Company), equipped with a temperature, pressure, and stirring

https://doi.org/10.1021/acsomega.3c07277
ACS Omega 2024, 9, 7793−7805

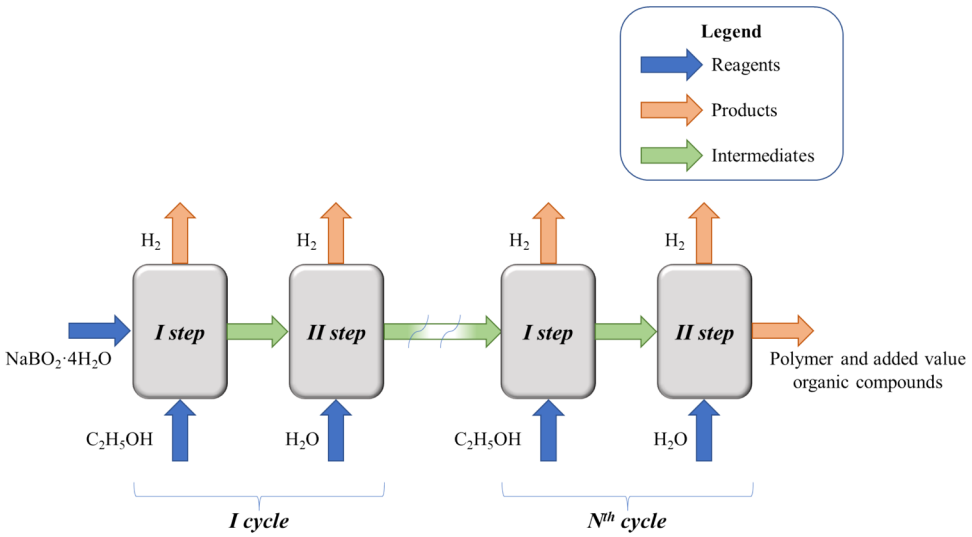

Figure 4. Block diagram of the cyan H_2 production process. The process consists of multiple cycles, each composed of two steps, and involves the alternated feeding of ethanol and water while maintaining a fixed initial amount of sodium metaborate. As a result, hydrogen is produced in the gas phase, while the liquid/solid products contain most of the fed carbon.

rate controller (model 4848, Parr Instrument Company). The experimental system diagram is reported in Figure S1.

The experimental protocol was designed to avoid the formation of explosive hydrogen−oxygen mixtures as follows: (i) loading of reagents (ethanol and sodium metaborate tetrahydrate and/or water) into the vessel and 12 inertization cycles with N_2; (ii) temperature (300 °C), heating rate (8 °C/min), and stirring speed (500 rpm) setting and test run until a pressure plateau was reached; (iii) end of the test, cooling at 60 °C, and gas sampling; (iv) cooling at room temperature and solid/liquid sampling.

Liquid/solid samples were separated by centrifugation at 12,000 rpm for 10 min (model SL 16R, Thermo Fisher Scientific, Inc.) and separately analyzed. Prior to analysis, the solid residue was washed and sonicated in ethanol and dried in a N_2 stream for 5 h at 50 °C. The experimental conditions adopted for each experimental run presented in this work are summarized in Table S1 (Supporting Information).

Gas Analysis. Gas samples were analyzed by means of a microgas chromatograph (GC) (microGC 3000, Agilent Technologies, Inc.) equipped with four independent modules each provided with a specific chromatographic column and a thermal conductivity detector (TCD). The injection temperature was set at 70 °C for each module, while a specific analysis temperature was set for each column. The column temperatures were 65, 90, 80, and 100 °C for OV-1, Alumina, PLOT U, and MS5A columns (Agilent columns), respectively. The carrier gas for OV-1, Alumina, and PLOT U columns was helium, while argon was used as a carrier in column MS5A. The injection volume was 10 μL. Gas sampling was carried out by means of 1 L bags with low hydrogen permeability. GC analysis was performed in triplicate.

Liquid Analysis. The identification of compounds was carried out by gas chromatography coupled to mass spectrometry (GC-MS). Qualitative liquid sample analysis was run by GC-MS (HP6890/HP5975, Agilent Technologies, Inc.) equipped with a DB-5MS capillary column (60 m × 0.25 mm ID), reaching the maximum temperature of 320 °C with a heating ramp of 10 °C/min. Chemical compounds were identified by comparing the mass spectra obtained with those of the system library. The relative abundance was assessed by dividing the peak area of a compound by the total area of the identified compounds.

Solid Analysis. Different analyses were carried out on the solid samples for both the identification and characterization of different properties. In particular, the solids were analyzed by Fourier transform infrared spectroscopy (FTIR), thermogravimetric analysis (TGA), X-ray powder diffraction (XRD), and matrix-assisted laser desorption/ionization combined with time-of-flight mass spectrometry (MALDI-TOF-MS) analysis.

The functional groups of the chemical structures were identified by FTIR analysis. We adopted an FTIR spectrometer (model Nicolet 5700, Thermo Electron Corporation) equipped with a DTGS KBr detector. FTIR spectra of all samples were recorded in the 4000−400 cm^{-1} range at a 2 cm^{-1} spectral resolution. Samples were prepared by mixing 199 mg of KBr and 1 mg of the dried sample and pressed into 13 mm pellets. The spectrum of each sample was corrected for that of blank KBr.

TG analysis (model Q600SDT TGA/DSC, TA Instruments) was carried out in a N_2 stream at a rate of 10 to 1000 °C/min to evaluate the thermal stability of the solid samples recovered during the process. Simultaneous FTIR gas analysis was carried out on the outlet gaseous stream to identify the degradation products. The cell and transfer line of the TGA/FTIR interface were heated and kept at 220 °C to prevent gas condensation. The output of this analysis was a Gram−Schmidt diagram. The HR Nicolet TGA Vapor Phase library of OMNIC software was used to recognize the produced gases.[30]

The chemical structure and crystallinity were evaluated by XRD analysis by an XRD diffractometer (model X'Pert Pro, Malvern PANalytical Ltd.) using Cu Kα radiation (1.5406 Å). The scanning range of 2θ was 5−100° with a step size of 0.013° and a scan step time of 18.87 s.

The in-depth investigation of the chemical structure (i.e., the repetitive unit) and the molecular weight of the solids was performed by means of MALDI-TOF-MS analysis (model 4800 ToF/ToF, Sciex). The samples were prepared for analysis from a fine suspension in ethanol or cyclohexane obtained by homogenization in an ultrasound bath. The

https://doi.org/10.1021/acsomega.3c07277
ACS Omega 2024, 9, 7793−7805

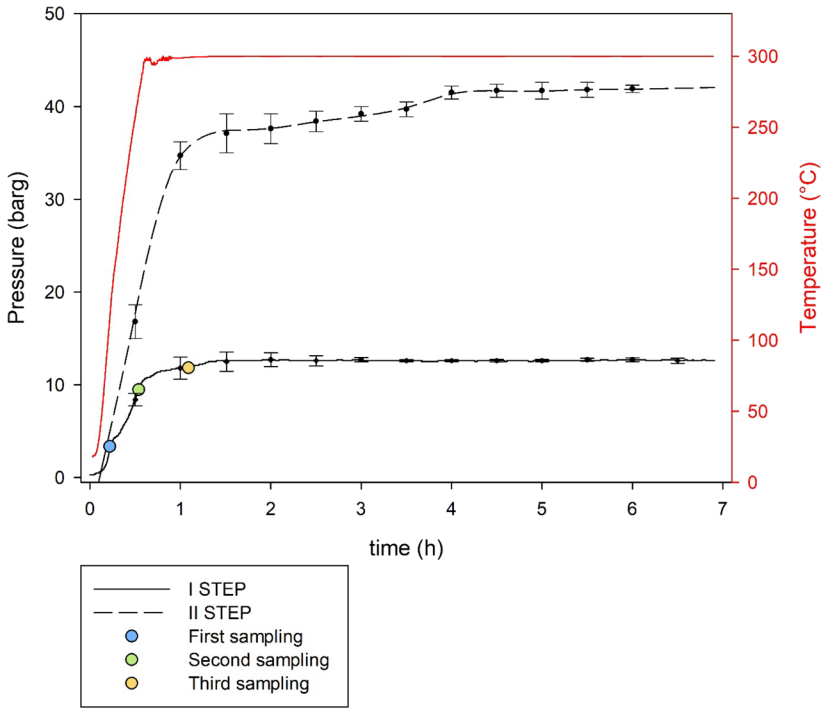

Figure 5. Temperature and pressure profiles as a function of time for steps I (5 mL of ethanol, 2.0 g of $NaBO_2{\cdot}4H_2O$) and II (H_2O, 10 mL) and intermediate collected samples at 0.41, 0.66, and 1.20 h during the I step.

Table 2. Volumetric Composition and Moles of Produced Gases during Each Step of the Process with 0.5, 1.0, and 2.0 g of $NaBO_2{\cdot}4H_2O$ as the Initial Amount, 5.0 mL of Ethanol during I and III Steps, and 10 mL of Water during II and IV Steps

	H_2		CO_2		*iso*-C_4H_{10}		ethylene	
process step	[%]	[mmol]	[%]	[mmol]	[%]	[mmol]	[%]	[mmol]
m_{NaBO2} = 0.5 [g] (3.62 [mmol])								
I step	89.32 ± 0.44	10.16 ± 0.05	8.23 ± 0.13	0.94 ± 0.01	0.99 ± 0.48	0.11 ± 0.05	1.46 ± 0.75	0.17 ± 0.08
II step	14.38 ± 1.44	1.87 ± 0.18	85.62 ± 2.33	11.13 ± 0.30	0.00	0.00	0.00	0.00
III step	27.29 ± 2.2	3.55 ± 0.28	72.71 ± 1.02	9.45 ± 0.13	0.00	0.00	0.00	0.00
IV step	23.56 ± 0.30	3.06 ± 0.04	76.44 ± 0.06	9.94 ± 0.01	0.00	0.00	0.00	0.00
m_{NaBO2} = 1.0 [g] (7.25 [mmol])								
I step	91.37 ± 2.04	13.37 ± 0.30	4.05 ± 0.30	0.59 ± 0.05	1.69 ± 1.11	0.225 ± 0.16	2.04 ± 0.9	0.30 ± 0.03
II step	94.84 ± 1.49	13.87 ± 0.22	0.99 ± 0.03	0.14 ± 0.01	3.33 ± 1.46	0.49 ± 0.21	0.00	0.00
III step	94.39 ± 1.69	12.27 ± 0.22	0.87 ± 0.01	0.11 ± 0.01	4.11 ± 0.80	0.53 ± 0.22	0.00	0.00
IV step	92.68 ± 0.72	12.05 ± 0.10	0.52 ± 0.16	0.07 ± 0.02	0.34 ± 0.04	0.044 ± 0.01	6.43 ± 0.79	0.84 ± 0.10
m_{NaBO2} = 2.0 [g] (14.50 [mmol])								
I step	94.83 ± 0.27	18.80 ± 0.04	1.67 ± 0.24	0.33 ± 0.03	3.47 ± 0.06	0.69 ± 0.01	0.00	0.00
II step	93.48 ± 0.21	11.80 ± 0.03	5.71 ± 0.16	0.72 ± 0.02	0.102 ± 0.07	1.3×10^{-02} ± 0.01	0.00	0.00
III step	98.56 ± 0.05	14.40 ± 0.007	1.09 ± 0.05	0.160 ± 0.007	0.00	0.00	0.20 ± 0.03	3.53×10^{-03} ± 0.01
IV step	95.2 ± 0.04	12.30 ± 0.006	2.54 ± 0.08	0.333 ± 0.01	0.00	0.00	0.70 ± 0.05	9.21×10^{-02} ± 0.01

solution of matrix CHCA (10 mg/mL) was prepared in an acetonitrile/water (1:1, v/v) mixture containing 0.1% TFA. One mL of the analyte (ethanol or cyclohexane) was premixed with 1 mL of the matrix in a centrifuge tube, and then, 2 μL of the resulting mixture was pipetted on the MALDI target plate and air-dried for MALDI-TOF-MS analysis. The laser was operated at 3700 Hz in the positive reflector mode. The mass spectrometer parameters were set as recommended by the manufacturer and adjusted for optimal acquisition performance. The laser spot size was set at medium focus (50 mm laser spot diameter). LDI (no matrix) spectra were also collected. The mass spectra data were acquired over a mass range of m/z 100−4000 Da, and each mass spectrum was collected from the accumulation of 1000 laser shots. Raw data were analyzed by using computer software provided by the manufacturers and reported as monoisotopic masses.

Simulation Methodologies. The equilibrium composition of products evolved during ethanol steam reforming at the same operating conditions of the cyan hydrogen production process was estimated with AspenPlus, using the RGibbs reactor model.[31]

RESULTS AND DISCUSSION

In the here proposed cyan H_2 production process, $NaBO_2{\cdot}4H_2O$ is upgraded by redox cycles to produce H_2 under mild conditions, i.e., at a low pressure and a relatively low

https://doi.org/10.1021/acsomega.3c07277
ACS Omega 2024, 9, 7793−7805

temperature (300 °C). The feedstock to the batch process consists of bioalcohols (in this case bioethanol), water, and $NaBO_2{\cdot}4H_2O$. The block diagram of the process is shown in Figure 4. In step I, ethanol (C_2H_5OH), hydration water, and sodium metaborate react, producing a gas stream at a high H_2 concentration and a liquid stream containing oxygenated organic compounds. The II step involves the addition of water, resulting in the formation of a second H_2-rich stream, a liquid residue containing organics, and a low-molecular-weight carbon−carbon chain product (oligomer). When the number of cycles (including I and II steps) is increased (from 2 to N), the molecular weight of the polymeric byproduct increases, without any significant change in the gaseous stream composition. The results of the experimental trials are discussed in detail below, and the experimental conditions are listed in Table S1.

I Step. In step I, 5.0 mL of C_2H_5OH (85.6 mmol) and 2.0 g of $NaBO_2{\cdot}4H_2O$ (14.5 mmol of $NaBO_2$ and 58.0 mmol of H_2O) are charged into the batch reactor. Starting from 0.3 barg of N_2 and 25 °C, the temperature is then increased to 300 °C.

In Figure 5, the black solid line represents the pressure profile of the I step, and a close examination of the curve reveals three different slopes. The pressure increase is due to the evaporation of ethanol, the temperature increase, and the generation of gaseous products and reaches a final value of 14.0 barg.

At the end of the process step, three different phases are obtained. The composition of the gaseous products sampled after cooling at 60 °C is reported in Table 2 (m_{NaBO2} = 2.0 g). Gas analysis shows a hydrogen composition of about 95% v/v and traces of other gases.

In the liquid phase collected after the I step, the main classes of organic compounds identified by GC-MS analysis are alcohols, aromatics, ketones, and aldehydes. In particular, the preliminary qualitative analysis shows the presence with relative abundance of 9.62% benzaldehyde (C_7H_6O), 27.07% 2-methyl-benzaldehyde (C_8H_8O), 24.96% 4-methyl-benzaldehyde (C_8H_8O), 10.22% (2-methyl-1-butenyl)-benzene ($C_{11}H_{14}$), 14.74% 1,3-bis(1,1-dimethylethyl)-benzene ($C_{14}H_{22}$), and 13.38% 2-methyl-benzenemethanol ($C_8H_{10}O$). Because of the complex composition, related to the abundance of organic compounds, detailed characterization requires refining and separation methods and is beyond the scope of the work. Future quantitative analyses may allow further investigation of the composition of the liquid phase.

FTIR analysis (Figure 6) was carried out on the solid phase recovered in each sampling to assess its composition. The FTIR spectrum shows weak and sharp bands at 2975 and 2929 cm^{-1} corresponding to CH_2 stretching and a strong and sharp band related to C═O at 1740 cm^{-1}. The doublet bands in the range of 1375−1450 cm^{-1} correspond to the symmetric and asymmetric bending for the CH_2 group.[32] The remaining bands (around 1000 cm^{-1}) can be related to sodium metaborate.[33] Thus, the FTIR spectrum suggests the formation of organic moieties trapped in the solid.

The presence of an organic phase in the solid is also highlighted by thermogravimetric analysis. Figure 7 shows the TG/DSC curves as well as the FTIR spectra of the gaseous product released during heating of the solid product recovered after the I step at 10 °C/min up to 1000 °C in N_2. The DSC curve (red solid line, Figure 7) shows endothermic peaks at 118 °C and one at 240 °C, accompanied by a mass change. The former can be ascribed to volatile loss (water and

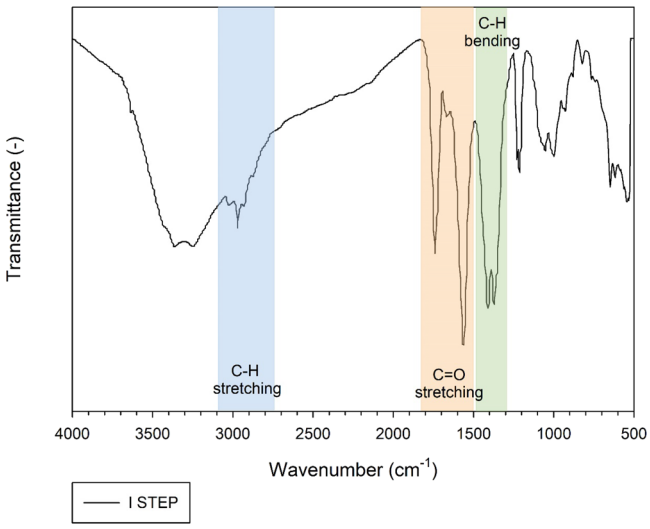

Figure 6. FTIR spectrum of the solid residue recovered after step I.

adsorbed organic compounds), as suggested by FTIR spectra of the gas phase, showing typical water absorption bands (at 3500 and 1630 cm^{-1}) as well as a broad halo in the range of 3023−2820 cm^{-1} featuring C−H stretching in organic moieties.[30] The spectra recorded at a temperature higher than 200 °C are typical of H_2O (3700−3500 and 1500−1300 cm^{-1} represent the −OH bond stretching vibrations in H_2O) and CO_2 (2400−2250 cm^{-1}) and suggest the decomposition of organic species in the sample.[34] The last endothermic peak, without a mass change, represented the melting of sodium metaborate, anticipated at 918 °C as it is in the mixed form.

II Step. During the II step, an additional 10 mL of H_2O (555.6 mmol) was added to the residue of the I step residue. The pressure profile and the gas analysis results are presented in Figure 5 (black dashed line) and Table 2 (m_{NaBO2} = 2.0 g), respectively.

Similarly to the I step, the pressure increases up to the plateau value of 42.0 barg, resulting in the production of a hydrogen-rich gaseous stream (about 94.0% v/v, Table 2).

GC-MS analysis of the liquid phase after the second step revealed with a high quality factor the presence of only 2-methyl-benzenemethanol ($C_8H_{10}O$), in contrast to the chemical richness of the liquid residue of step I. This could be related to the high water content of the residue, which leads to dilution of the system limiting the detection of less abundant moieties. Future analyses will be carried out on the refined liquid products in order to quantify these species.

The DSC curve (red dashed line, Figure 8A) on the solid residue from the II step shows an endothermic peak associated with either absorbed or structural water release at around 120 °C, which was less intense than that recorded for the solid recovered after step I. Thus, considering the weight loss from 200 °C, a 26% organic content was estimated at the end of step II. More specifically, the weight loss occurs in three different phases: up to 400 °C, there is a weight loss of 23%, from 400 to 480 °C, there is a loss of 9.3% much faster than the previous one, and up to 1000 °C, there is a gradual loss of 7.6%. As reported in Figure 8B, the linked spectrum at 160 °C, collected on the gaseous species evolved during the initial weight loss, does not exhibit any absorbance peaks related to CH_2 bond vibrations, thus suggesting that no organic compound was released from the sample in that temperature range. On the

https://doi.org/10.1021/acsomega.3c07277
ACS Omega 2024, 9, 7793−7805

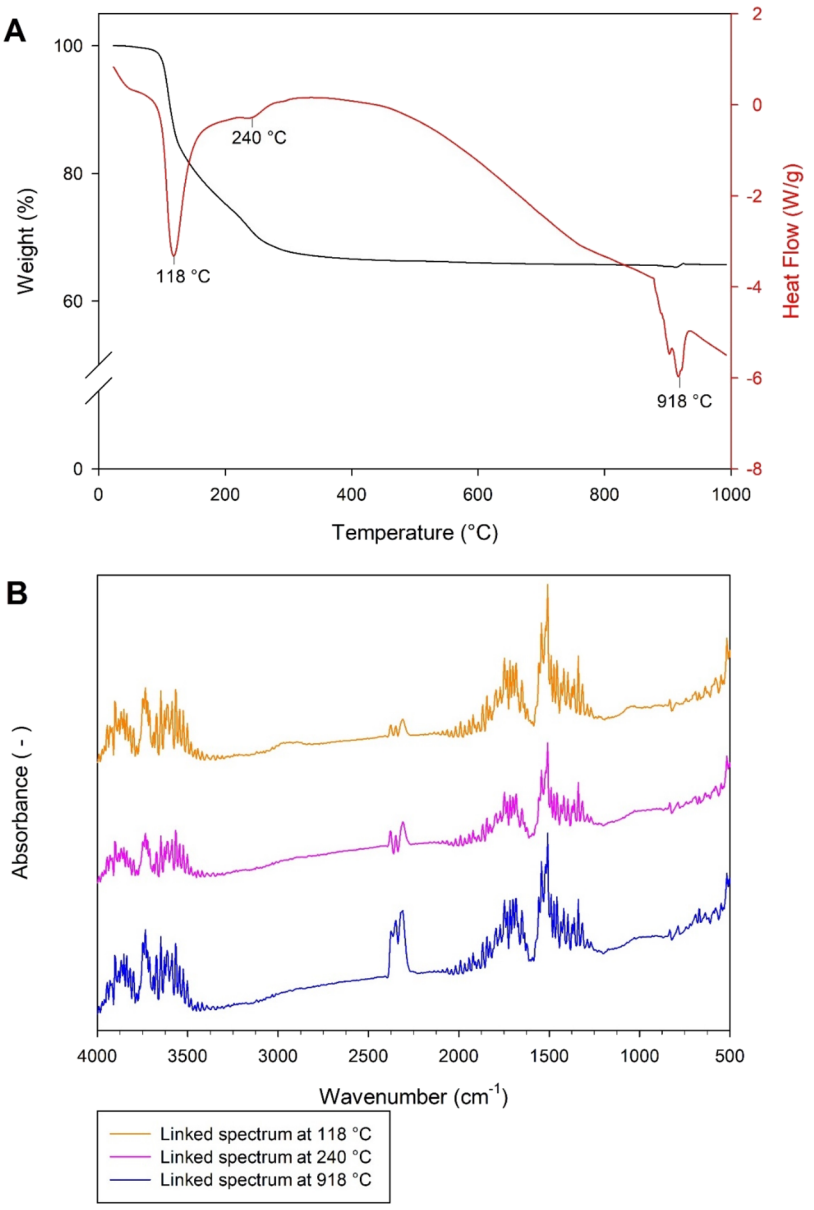

Figure 7. TG/DSC (A) of the I step solid residue and (B) FTIR spectra of evolved gases with a temperature ramp of 10 °C/min up to 1000 °C in nitrogen flow.

other hand, during the second weight loss, the spectrum at 455 °C shows CH_2 stretching modes (3020−2810 cm^{-1}), while during the last stage, the spectrum at 830 °C identifies CO_2 in the 2400−2250 cm^{-1} range with peaks at 2357 and 2308 cm^{-1} and CO in the 2220−2060 cm^{-1} range with peaks at 2177 and 2108 cm^{-1}.[35] Comparing TG-FTIR results of solids after steps I (Figure 7B) and II (Figure 8B), it can be argued that the thermal decomposition of organic compounds in the latter sample is shifted to a higher temperature than the values recorded on the former. Notably, decomposition of samples recovered after STEP I tends at 300 °C (offset temperature). On the other hand, for a solid obtained after the II step, the largest weight loss stops at 500 °C, but a slow thermal evolution continues also up to 1000 °C. This suggests that the molecular weight of the organic fraction increases during step II. In addition, the thermal stability of the formed organic oligomer could be improved by the presence of inorganic borate, which is recognized as a very effective stabilizer for thermal degradation.[36] In fact, due to the presence of the boron compound that acts as a thermal and mechanical stabilizer,[37] the oligomer/polymer can withstand 300 °C.

Double Cycle. To preliminarily assess the cyclability of the process and the effect of the number of steps on the produced polymer, steps I and II were repeated two times, with the consecutive addition of ethanol and water, purging, and analyzing the gaseous products obtained between the runs.

Pressure increases with the same trend as that in the I step during each consecutive step and reaches increasing values as the number of steps increases, as outlined in Table S1.

The hydrogen volumetric content in the gas phase remains almost constant in the different steps (Table 2, m_{NaBO2} = 2.0 g). However, in the liquid phase, high dilution does not allow the identification of other species beyond 2-methyl-benzene-methanol.

Figure 9 shows FTIR spectra of the solid residue recovered after a double cycle (solid green line), suggesting the presence

https://doi.org/10.1021/acsomega.3c07277
ACS Omega 2024, 9, 7793−7805

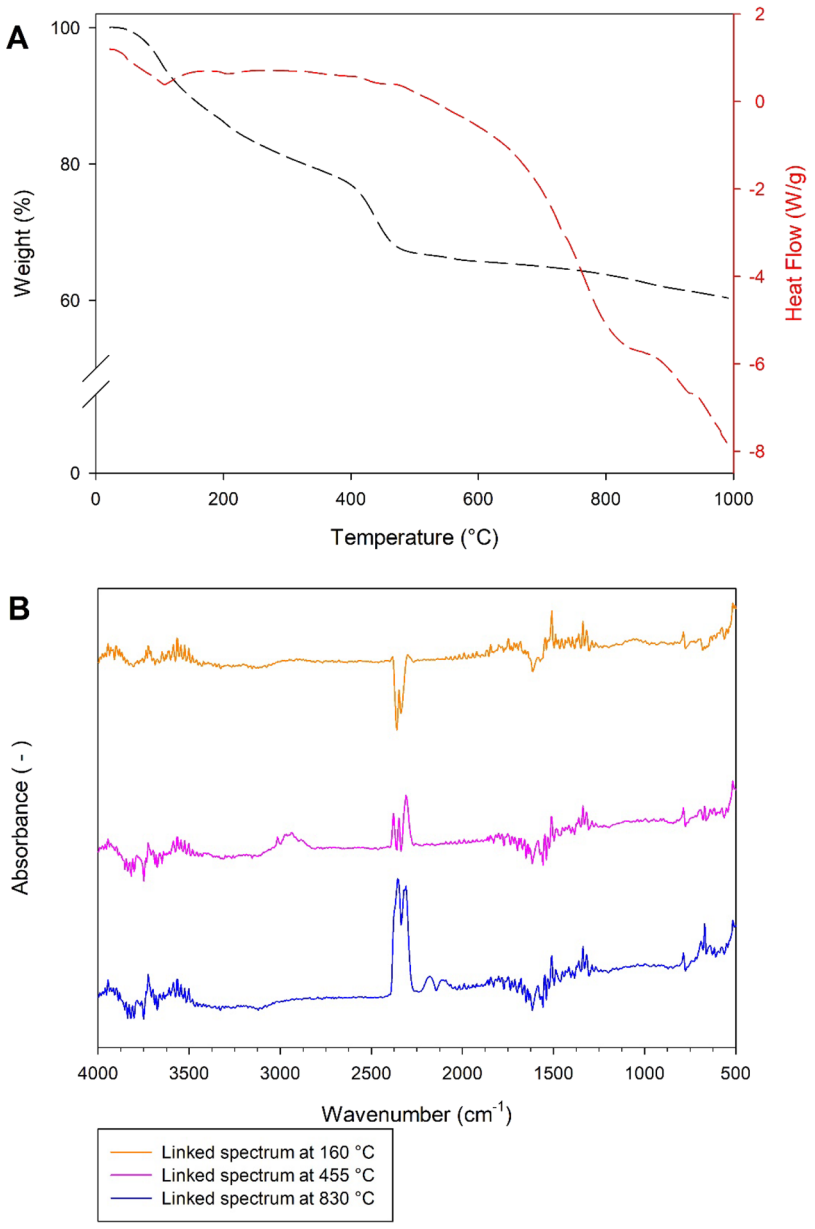

Figure 8. TG/DSC (A) of the II step solid residue and (B) FTIR spectra of evolved gases with a temperature ramp of 10 °C/min up to 1000 °C in nitrogen flow.

of boric acid (2615 and 2441 cm^{-1}), sodium metaborate (1660, 1276, and 1131 cm^{-1}), and organic moieties (bands at 2800−3000 cm^{-1}), more evident in the samples with less $NaBO_2$ content.

The presence of organic matter in the solid residue after a double cycle was further supported by MALDI-TOF-MS analysis (Figure S2), which detected a repetitive carbon pattern of 28 uma, i.e., the mass of $-CH_2-CH_2-$, a feature of alkanes, typical of polyethylene. Such a C2 unit presents an overall oxidation state for the carbon of −2, the same for the two carbon atoms in the source ethanol. In this perspective, its formation can be interpreted in terms of water loss associated with coupling of ethanol[38] molecules resulting in an oligomer/polymer, according to the following Scheme 1 for the solid phase. Also, the average molar mass determined is about 100−300 Da, indicating the formation of a macromolecule. Several end-capping structures can be hypothesized, such as cyclic or heterocyclic systems, but it is difficult to conclusively propose a given structure for the observed mass patterns without further investigations.

As a result, the following is a schematization of the lumped reaction of the cyan hydrogen production process. The process involves the following two steps:

$$\mathbf{I}^{(1)})\ NaBO_2{\cdot}4H_2O_{(s)} + C_2H_5OH_{(l)} \rightarrow S^{(I(1))}{}_{(s)} + L^{(I(1))}{}_{(l)} + H_{2(g)}$$

$$\mathbf{II}^{(1)})\ S^{(I(1))}{}_{(s)} + L^{(I(1))}{}_{(l)} + H_2O_{(l)} \rightarrow NaBO_2{\cdot}xH_2O_{(s)} + H_{2(g)} + S^{(II(1))}{}_{(s)} + L^{(II(1))}{}_{(l)} + PM^{(II(1))}{}_{(s)}$$

and at least one cycle (i) after the first two steps:

$$\mathbf{I}^{(i)})\ NaBO_2{\cdot}xH_2O_{(s)} + S^{(II(i-1))}{}_{(s)} + L^{(II(i-1))}{}_{(l)} + PM^{(II(i-1))}{}_{(s)} + C_2H_5OH_{(l)} \rightarrow S^{(I(1))}{}_{(s)} + L^{(I(1))}{}_{(l)} + H_{2(g)}$$

$$\mathbf{II}^{(i)})\ S^{(I(i))}{}_{(s)} + L^{(I(i))}{}_{(l)} + PM^{(I(i))}{}_{(s)} + H_2O_{(l)} \rightarrow NaBO_2{\cdot}xH_2O_{(s)} + PM^{(II(i))}{}_{(s)} + H_{2(g)} + S^{(II(i))}{}_{(s)} + L^{(II(i))}{}_{(l)}$$

where

- i ranges from 2 to N and N is the total number of cycles;

https://doi.org/10.1021/acsomega.3c07277
ACS Omega 2024, 9, 7793−7805

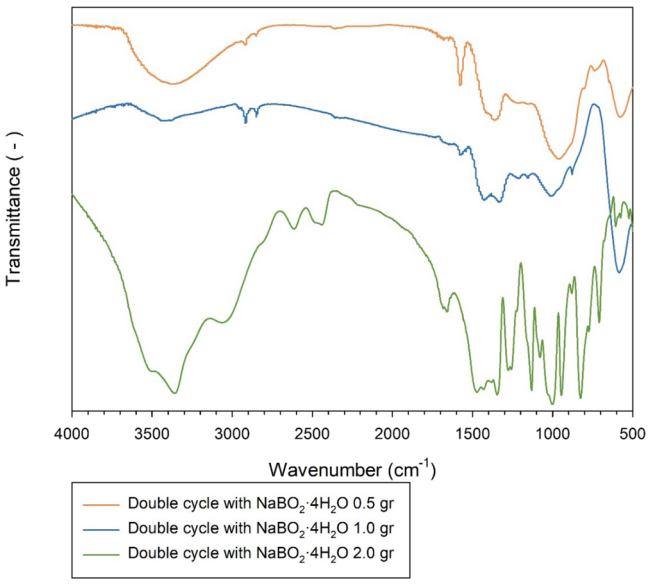

Figure 9. FTIR spectra of the double-cycle solid residue with 0.5, 1.0, and 2.0 g of sodium metaborate tetrahydrate (orange, blue, and green solid lines, respectively).

- S(s) represents an intermediate solid consisting of a mixture of Na and B compounds, such as $Na_2B_4O_7$ hydrate or not, and organic compounds;
- L(s) represents an intermediate liquid consisting mainly of organic compounds of an aliphatic and aromatic nature;
- PM $^{(\mathrm{II}(i))}_{(s)}$ is a polymeric compound, the molecular weight of which increases as the number of cycles increases, and when i = 1, it is the relevant polymer precursor, such as a monomer, dimer, or oligomer;
- x is the number of water molecules of hydration of the metaborate, between 1 and 4.

This proposed schematization considers the preliminary characterization of the multiphase products, as thorough quantitative characterization of liquid and solid phases is beyond the scope of this article. Future analyses of the reaction products and intermediates in the different phases will clarify the reaction mechanism and detail all of the species produced during the reaction. Figure 10 depicts the overall scheme of the process, reporting the main component of each phase at the end of the process. As mentioned above, the purity grade of the hydrogen stream is kept almost constant in the range of 94–99% v/v. The liquid phase, on the other hand, is rich in oxygenated compounds; among these, the one detected in each liquid sample is 2-methyl-benzenemethanol (also known as benzyl alcohol). This compound is utilized in cosmetics as a fragrance, in human medicine as an antimicrobial preservative and local anesthetic, as a solvent for paints, glues, and adhesives,[39] and as a food additive.[40] Benzaldehyde hydrogenation and benzyl chloride hydrolysis are the main processes to produce benzyl alcohol for industrial use, which involve the use of nonrenewable substrates, high temperatures, and byproducts that have a negative impact on the environment.[41] As summarized in Figure 10, the solid phase consists of a mixture of low-molecular-weight oligomers/polymers with the structure $-CH_2-CH_2-$ mixed with boron compounds. Although high-molecular-weight polyethylene has been widely used as thermoplastics throughout the world, low-molecular-weight ethylene oligomers can also fulfill numerous functions. In particular, the focus is on either linear waxlike oligoethylenes, most obtained via the Ziegler Alfol synthesis, or branched amorphous oligomers that can also be used as synthetic lubricants, active interface agents, or viscosity modifiers.[42,43]

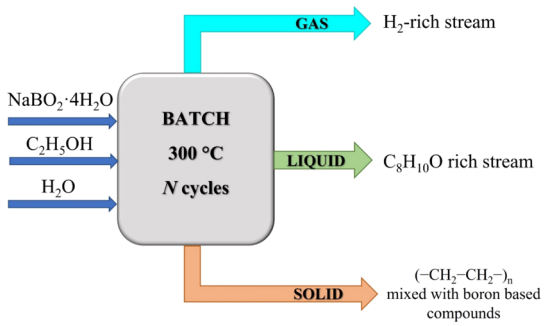

Figure 10. Qualitative scheme of the process showing the reagents and the main products of each phase.

In order to assess the performance and feasibility of the process and compare it with the currently most widely used adopted hydrogen production method, i.e., ethanol steam reforming, the performance indexes I_1 and I_2 were defined as shown in the following equations (eqs 2 and 3):

$$I_1 = \frac{n_{\mathrm{H_2,produced}}}{3 \times n_{\mathrm{C_2H_5OH,inlet}}} \times 100 \quad (2)$$

$$I_2 = \frac{n_{\mathrm{H_2,produced}}}{n_{\mathrm{CO_2,produced}}} \quad (3)$$

Since the reaction stoichiometry is currently unknown and under investigation, the performance indicator is calculated on the basis of the atomic balance with respect to ethanol, i.e., the highest-value reagent.

Considering the initial steps of the process, the indicator I_1 was 7.31 and 11.91% for the I and II step, respectively. It is important to consider that the overall cycle performance achieved during the cyan hydrogen production process is about 12%, under not yet optimized process conditions. It is worth noting that hydrogen atoms of bioethanol are split into (i) gaseous hydrogen, (ii) hydrogen of $-CH_2-$polymer units, and (iii) hydrogen contained in liquid organic compounds, thus

Scheme 1. Proposed Reaction Scheme for the Solid Phase

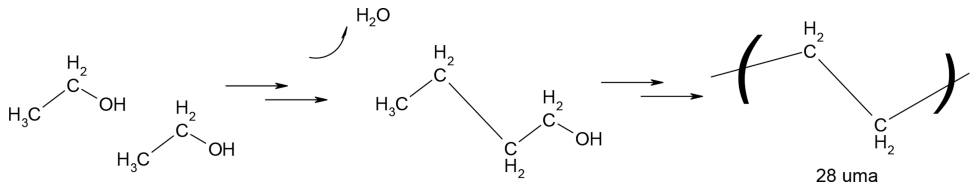

https://doi.org/10.1021/acsomega.3c07277
ACS Omega 2024, 9, 7793–7805

Table 3. Volumetric Composition and Moles of Produced Gases during the Intermediate Collected Samples at 0.41, 0.66, and 1.20 h of the I Step with 2.0 g of $NaBO_2{\cdot}4H_2O$ and 5.0 mL of C_2H_5OH

	H_2		CO_2		*iso*-C_5H_{12}		*iso*-C_4H_{10}	
process step	[%]	[mmol]	[%]	[mmol]	[%]	[mmol]	[%]	[mmol]
first sampling	16.52 ± 1.3	2.69 ± 0.19	25.31 ± 2.2	4.11 ± 0.32	48.30 ± 2.5	7.85 ± 0.19	9.87 ± 1.4	1.60 ± 0.21
second sampling	59.80 ± 1.7	8.64 ± 0.25	25.98 ± 0.40	3.75 ± 0.06	13.84 ± 0.26	2.00 ± 0.04	0.39 ± 0.24	0.056 ± 0.03
third sampling	82.23 ± 0.95	13.36 ± 0.14	12.08 ± 0.14	1.96 ± 0.02	5.14 ± 0.73	0.84 ± 0.10	0.53 ± 0.37	0.087 ± 0.05
I step	94.83 ± 0.57	18.8 ± 0.08	1.67 ± 0.03	0.33 ± 0.005	0.00	0.00	3.47 ± 0.62	0.69 ± 0.09

explaining the low value of the overall cycle performance index. Moreover, hydrogen is produced in the pressure range of 15−45 barg, making this process convenient for direct entry of the produced gas, postpurification, into pipelines.

To contextualize the cyan hydrogen process in the current scenario of hydrogen production from bioethanol, the performance index I_1 was calculated for ethanol steam reforming reaction under the same operating conditions, i.e., 300 °C, 1 bar, and H_2O/ethanol = 7. From a thermodynamic point of view, the performance index achieves 13.3%. Under such temperature conditions, only limited data can be found in the literature for the hydrogen yield of ethanol steam reforming in the presence of a catalyst.[44] Furthermore, the data found in the literature are discouraging on the steam reforming process of ethanol at 300 °C due to the high formation of coke and catalyst deactivation.[45] Moreover, considering the I_2 index as a measure of gas stream selectivity, it can be seen that against the 0.66 value of conventional ethanol steam reforming, cyan hydrogen is the predominant product with an I_2 equal to 26.

Effect of the Sodium Metaborate Amount. To study the role of sodium metaborate in the process, cyclability tests (i.e., double cycles) were carried out for different initial amounts of metaborate, specifically 0.5, 1.0, and 2.0 g, keeping the H_2O/ethanol feed ratio constant in the I step. It is worth noting that in the I step, water was already present in the reagent (sodium metaborate tetrahydrate), and further distilled water was added to keep the ratio constant.

The results of microGC analysis of the gas samples are shown in Table 2 for the different tests. For the largest amount of sodium metaborate fed (i.e., 2.0 g), the hydrogen volumetric fraction increases and remains almost constant in the different steps. The same trend is shown for the intermediate metaborate amount, i.e., 1.0 g, but the hydrogen content changes in the range of 92−95%, lower than for higher metaborate contents (94−99%). On the other hand, in the case of 0.5 g of $NaBO_2{\cdot}4H_2O$, a significant variation in the gas composition of the different steps was observed, going from about 89% hydrogen in the I step to about 24% in the IV step. More specifically, when 0.5 g of $NaBO_2{\cdot}4H_2O$ was used, the stream was rich in CO_2. As a result, as sodium metaborate increases, the gas stream becomes purer in hydrogen, presenting only a low concentration of CO_2 and other species. This could indicate that for low amounts of metaborate, high efficiency in the CO_2 decrement and hydrogen production reaction is not achieved.

In Figure 9, the spectrum of the double-cycle solid residue with 0.5 g of $NaBO_2{\cdot}4H_2O$ (orange solid line) shows two sharp bands of weak intensity at 2917 and 2851 cm^{-1}, assigned to the asymmetric and symmetric stretching vibrations of $-CH_2$, respectively. Furthermore, the strong absorption band at 1558 cm^{-1} is attributed to the asymmetric stretching vibration of the single bond $-COO^-$ group.[46,47] The same bands at 2917 and 2851 cm^{-1} with medium intensity are visible in the spectrum of the double cycle with 1.0 g of $NaBO_2{\cdot}4H_2O$ (blue solid line), while the O−H bond stretching band in the 2.0 g case covers the signal. The double-cycle spectrum shows bands in common with boric acid (2615 and 2441 cm^{-1}) and sodium metaborate itself (1660, 1276, and 1131 cm^{-1}), and bands at 1413 and 1344 cm^{-1} were due to the C−H bending vibrations, like the spectra of the I step (Figure 6).

I Step: Focus on Carbon Valorization. During the heating, the pressure profile of the I step (black solid line, Figure 5) shows three slope changes; therefore, three gas samples were taken before each variation. The operating conditions of intermediate sampling of the I step are first sampling at 0.41 h and 170 °C, second sampling at 0.66 h and 300 °C, and third sampling at 1.20 h and 300 °C, represented by highlighted dots in blue, green, and yellow in Figure 5, respectively.

The initial pressure increase is ascribable to the ethanol and water vaporization and then to temperature increases, and gaseous products are generated, reaching a final pressure of 14.0 barg. More in details, the slope changes are respectively associated with ethanol evaporation, CO_2 and H_2 production, and a CO_2 decrease and further H_2 production, respectively.

The gas analysis reported in Table 3 shows that the reaction initially evolves with a significant formation of CO_2 in the gas phase and other intermediates, such as isopentane (C_5H_{12}) and butane (C_4H_{10}). Then, their concentration decreases with time with the simultaneous hydrogen enrichment, reaching a final hydrogen composition of about 95% v/v.

Oxygenated aromatic species present at the end of step I are detected in the liquid phase but with a smaller associated area in the chromatographic spectrum.

The FTIR spectra of the intermediate solid residue samples of the I step are shown in Figure 11 (blue, green, and yellow solid lines) compared with I step spectra (black solid line). The spectra collected during the initial phase of the I step show O−H stretching, H−O−H bending, B−O−H bending, and the asymmetric and symmetric B−O stretching bands at 3292, 1669, 1263, 1128, and 879 cm^{-1}, respectively, as the $NaBO_2{\cdot}4H_2O$ bare spectrum.[48] The spectra of the intermediate samples overlap with the sodium metaborate spectrum (red solid line, Figure 11), thus indicating that metaborate remains unreacted in the initial phase of the reaction, while the spectra of the I step show the organic compound presence (as reported in Figure 6). Confirming this, XRD analyses (Figure S3) show that the peaks for the intermediate samples are related to sodium borate dihydrate ($NaB(OH)_4{\cdot}2H_2O$, PDF no. 01-076-0756), i.e., the molecular structure of metaborate tetrahydrate.

So, while sodium metaborate does not change during the initial stage of the reaction, carbon initially present in ethanol shows an interesting course: CO_2 is produced in the initial

https://doi.org/10.1021/acsomega.3c07277
ACS Omega 2024, 9, 7793−7805

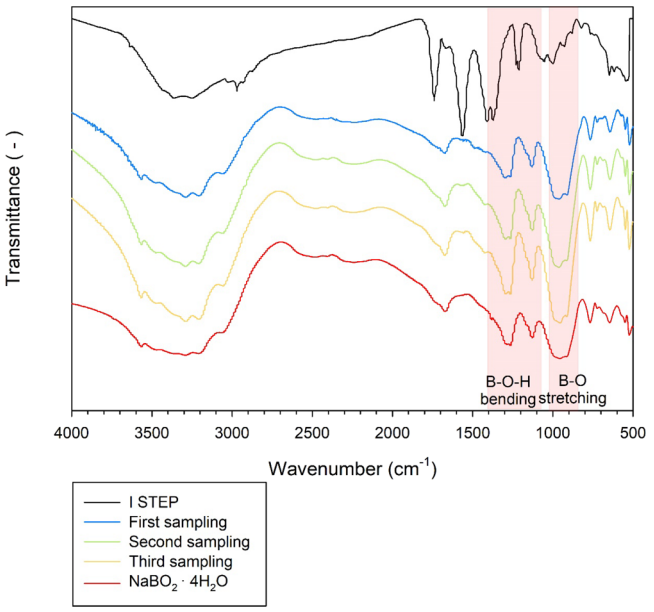

Figure 11. FTIR spectra of the I step (black solid line) and intermediate solid residues (blue, green, and yellow solid lines) collected during the I step, compared to bare $NaBO_2 \cdot 4H_2O$ (red solid line).

phase but then decreases to a max. value of 5% by volume in the gas stream, and at the end of the process, carbon is in the solid phase as an oligomer/polymer and in the liquid phase as organic chemicals.

CONCLUSIONS

The present study shows the preliminary results of a novel hydrogen production process, here named for the first time cyan H_2, due to the inspiration given by the low content of carbonaceous gases in blue hydrogen and water adoption in green H_2.

The proof of concept of the developed process consists of alternate cycles in the presence of bioethanol, water, and sodium metaborate tetrahydrate at 300 °C and allows the simultaneous production of hydrogen-rich gas (>95%), oligomeric/polymeric products (polyethylene in the case of bioethanol), and a liquid phase rich in organic compounds.

Investigating the evolution of carbon species in the gaseous phase during the process, it was observed that carbon dioxide was produced at an early intermediate stage and then during the reaction decreases, while the hydrogen amount increases, resulting ultimately in a H_2-rich gas phase. The preliminary results show that the carbon initially fed with ethanol is valorized, giving interesting byproducts such as benzyl alcohol in the liquid phase, which is widely used in cosmetics, medicine, and food fields. Instead, a polymeric compound with a repetitive carbon pattern of 28 uma, i.e., the mass of $-CH_2-CH_2-$ and mass of 100−300 Da in the solid phase.

The advantages of the here proposed cyan hydrogen production process are

- use of borates, byproducts derived from the dehydrogenation of boron hydrides used for hydrogen storage and that are very difficult to regenerate;
- production of a 95% v/v hydrogen stream;
- less than 4% v/v carbon dioxide in the gaseous stream;
- valorization of the carbon fed to a polymeric product and to liquid organic compounds;
- mild operating conditions (temperature of about 300 °C).

Our findings highlight the possibility of using bioderived and cheap waste materials for a cost-effective and environmentally friendly hydrogen production process, with simultaneous carbon valorization and fine chemical production. Future optimization will lay the groundwork for process implementation. Further investigations will clarify the role of intermediates, and the thorough quantitative characterization of condensed phases and product distribution will allow the understanding of the reaction mechanism and highlight the possibility to adopt other biorefinery chemicals as process feedstocks.

ASSOCIATED CONTENT

Supporting Information

The Supporting Information is available free of charge at https://pubs.acs.org/doi/10.1021/acsomega.3c07277.

- Experimental system diagram (Figure S1), MALDI spectrum of the double-cycle solid residue (Figure S2), XRD spectra of the intermediate sampling solid residue (Figure S3), and experimental conditions for each test (Table S1) (PDF)

AUTHOR INFORMATION

Corresponding Author

Almerinda Di Benedetto − *Department of Chemical, Materials and Production Engineering, University of Naples Federico II, Naples 80125, Italy;* orcid.org/0000-0002-3809-0369; Email: almerinda.dibenedetto@unina.it

Authors

Alessandra Di Nardo − *Department of Chemical, Materials and Production Engineering, University of Naples Federico II, Naples 80125, Italy;* orcid.org/0000-0003-1913-0414

Maria Portarapillo − *Department of Chemical, Materials and Production Engineering, University of Naples Federico II, Naples 80125, Italy;* orcid.org/0000-0002-7463-6154

Danilo Russo − *Department of Chemical, Materials and Production Engineering, University of Naples Federico II, Naples 80125, Italy;* orcid.org/0000-0003-1809-7309

Giuseppina Luciani − *Department of Chemical, Materials and Production Engineering, University of Naples Federico II, Naples 80125, Italy;* orcid.org/0000-0002-1169-0137

Gianluca Landi − *Istituto di Scienze e Tecnologie per l'Energia e la Mobilità Sostenibili (STEMS), Consiglio Nazionale delle Ricerche, Naples 80125, Italy*

Giovanna Ruoppolo − *Istituto di Scienze e Tecnologie per l'Energia e la Mobilità Sostenibili (STEMS), Consiglio Nazionale delle Ricerche, Naples 80125, Italy*

Alessandro Pezzella − *Department of Physics "Ettore Pancini", University of Naples Federico II, Complesso Universitario Monte S. Angelo, Naples 80126, Italy;* orcid.org/0000-0001-6925-922X

Complete contact information is available at: https://pubs.acs.org/10.1021/acsomega.3c07277

Author Contributions

A.D.N. performed experimental investigation, data curation, formal analysis, experimental setup design, methodologies,

https://doi.org/10.1021/acsomega.3c07277
ACS Omega 2024, 9, 7793−7805

analytics, writing of the original draft, and review and editing of the manuscript. M.P.performed experimental investigation, methodologies, analytics, writing of the original draft, and review and editing of the manuscript. D.R. performed formal analysis, methodologies, analytics, and review and editing of the manuscript; G.Luciani and G.Landi performed experimental setup design, methodologies, analytics, supervision, and review and editing of the manuscript. G.R. performed analytics and data curation. A.P. performed formal analysis, analytics, and review and editing of the manuscript. A.D.B. performed experimental setup design, methodologies, conceptualization, formal analysis, funding acquisition, project administration, supervision, writing of the original draft, and review and editing of the manuscript.

Funding

This research did not receive any specific grant from funding agencies in the public, commercial, or not-for-profit sectors.

Notes

The authors declare no competing financial interest.

■ ACKNOWLEDGMENTS

The authors acknowledge Mr. Fernando Stanzione for his technical support.

■ REFERENCES

(1) Mohan, S. V.; Katakojwala, R. The Circular Chemistry Conceptual Framework: A Way Forward to Sustainability in Industry 4.0. *Curr. Opin Green Sustain Chem.* **2021**, *28*, 100434.

(2) Masson-Delmotte, V.; Zhai, P.; Pörtner, H.-O.; Roberts, D.; Skea, J.; Shukla, P. R.; Pirani, A.; Moufouma-Okia, W.; Péan, C.; Pidcock, R.; Connors, S.; Matthews, J. B. R.; Chen, Y.; Zhou, X.; Gomis, M. I.; Lonnoy, E.; Maycock, T.; Tignor, M.; Waterfield, T. IPCC Summary for Policymakers. In: *Global Warming of 1.5°C. An IPCC Special Report on the Impacts of Global Warming of 1.5°C above Pre-Industrial Levels and Related Global Greenhouse Gas Emission Pathways, in the Context of Strengthening the Global Response to the threat of climate change, sustainable development, and efforts to eradicate poverty*. World Meteorological Organization: Geneva, Switzerland, 2018 32 DOI: 10.1017/9781009157940.001.

(3) Tan, W.CNBC. *What 'transition'? Renewable energy is growing, but overall energy demand is growing faster*. https://www.cnbc.com 2021.

(4) Elam, C. C.; Padró, C. E. G.; Sandrock, G.; Luzzi, A.; Lindblad, P.; Hagen, E. F. Realizing the Hydrogen Future: The International Energy Agency's Efforts to Advance Hydrogen Energy Technologies. *Int. J. Hydrogen Energy* **2003**, *28* (6), 601−607.

(5) Okolie, J. A.; Epelle, E. I.; Tabat, M. E.; Orivri, U.; Amenaghawon, A. N.; Okoye, P. U.; Gunes, B. Waste Biomass Valorization for the Production of Biofuels and Value-Added Products: A Comprehensive Review of Thermochemical, Biological and Integrated Processes. *Process Safety and Environmental Protection* **2022**, *159*, 323−344.

(6) Tee, S. Y.; Win, K. Y.; Teo, W. S.; Koh, L. D.; Liu, S.; Teng, C. P.; Han, M. Y. Recent Progress in Energy-Driven Water Splitting. *Adv. Sci.* **2017**, *4* (5), 1600337.

(7) Younas, M.; Shafique, S.; Hafeez, A.; Javed, F.; Rehman, F. An Overview of Hydrogen Production: Current Status, Potential, and Challenges. *Fuel* **2022**, *316*, 123317.

(8) EWE. *The colours of hydrogen*, https://www.ewe.com.

(9) Ajanovic, A.; Sayer, M.; Haas, R. The Economics and the Environmental Benignity of Different Colors of Hydrogen. *Int. J. Hydrogen Energy* **2022**, *47* (57), 24136−24154.

(10) Arcos, J. M. M.; Santos, D. M. F. The Hydrogen Color Spectrum: Techno-Economic Analysis of the Available Technologies for Hydrogen Production. *Gases* **2023**, *3* (1), 25−46.

(11) International Energy Agency. *Global Hydrogen Review 2022*, 2022, www.iea.org/t&c/.

(12) International Energy Agency. *The Future of Hydrogen- Seizing Today's Opportunities: Reported Prepared by the IEA for the G20*; 2019.

(13) Bauer, C.; Treyer, K.; Antonini, C.; Bergerson, J.; Gazzani, M.; Gencer, E.; Gibbins, J.; Mazzotti, M.; McCoy, S. T.; McKenna, R.; Pietzcker, R.; Ravikumar, A. P.; Romano, M. C.; Ueckerdt, F.; Vente, J.; van der Spek, M. On the Climate Impacts of Blue Hydrogen Production. *Sustain Energy Fuels* **2021**, *6* (1), 66−75.

(14) Hermesmann, M.; Müller, T. E. Green, Turquoise, Blue, or Grey? Environmentally Friendly Hydrogen Production in Transforming Energy Systems. *Prog. Energy Combust. Sci.* **2022**, *90*, 100996.

(15) IEA. *Hydrogen Production Costs Using Natural Gas in Selected Regions, 2018*; 2019. https://www.iea.org/data-and-statistics/charts/hydrogen-production-costs-using-natural-gas-in-selected-regions-2018-2.

(16) Oliveira, A. M.; Beswick, R. R.; Yan, Y. A Green Hydrogen Economy for a Renewable Energy Society. *Curr. Opin Chem. Eng.* **2021**, *33*, 100701.

(17) Zhou, Y.; Li, R.; Lv, Z.; Liu, J.; Zhou, H.; Xu, C. Green Hydrogen: A Promising Way to the Carbon-Free Society. *Chin J. Chem. Eng.* **2022**, *43*, 2−13.

(18) Korányi, T. I.; Németh, M.; Beck, A.; Horváth, A. Recent Advances in Methane Pyrolysis: Turquoise Hydrogen with Solid Carbon Production. *Energies.* **2022**, *15*, 6342.

(19) Di Benedetto, A.; Portarapillo, M.; Landi, G.; Luciani, G. Process for Green Hydrogen Production. WO2023105545A1, 2023.

(20) Kanturk, A.; Sari, M.; Piskin, S. Synthesis, Crystal Structure and Dehydration Kinetics of $NaB(OH)_4{\cdot}2H_2O$. *Korean J. Chem. Eng.* **2008**, *25*, 1331.

(21) Garret, E. D. *Borates, Handbook of Deposits, Processing, Properties and Use*, Academic Press: California, USA, 1998.

(22) Nunes, H. X.; Silva, D. L.; Rangel, C. M.; Pinto, A. M. F. R. Rehydrogenation of Sodium Borates to Close the NaBH4-H2 Cycle: A Review. *Energies* **2021**, *14*, 1−28.

(23) Ferreira, M. J. F.; Gales, L.; Fernandes, V. R.; Rangel, C. M.; Pinto, A. M. F. R. Alkali Free Hydrolysis of Sodium Borohydride for Hydrogen Generation under Pressure. *Int. J. Hydrogen Energy* **2010**, *35* (18), 9869−9878.

(24) Demirci, U. B.; Akdim, O.; Miele, P. Ten-Year Efforts and a No-Go Recommendation for Sodium Borohydride for on-Board Automotive Hydrogen Storage. *Int. J. Hydrogen Energy* **2009**, *34* (6), 2638−2645.

(25) Kojima, Y.; Haga, T. Recycling Process of Sodium Metaborate to Sodium Borohydride. *Int. J. Hydrogen Energy* **2003**, *28* (9), 989−993.

(26) Melikoglu, M.; Singh, V.; Leu, S.-Y.; Webb, C.; Lin, C. S. K. 9 - Biochemical Production of Bioalcohols. In *Handbook of Biofuels Production* (Second Edition); Luque, R., Lin, C. S. K., Wilson, K., Clark, J., Eds.; Woodhead Publishing, 2016; pp 237−258. DOI: 10.1016/B978-0-08-100455-5.00009-6.

(27) Scully, S. M.; Orlygsson, J. Chapter 5 - Biological Production of Alcohols. In *Advanced Bioprocessing for Alternative Fuels, Biobased Chemicals, and Bioproducts*; Hosseini, M., Ed.; Woodhead Publishing Series in Energy; Woodhead Publishing, 2019; pp 83−108. DOI: 10.1016/B978-0-12-817941-3.00005-X.

(28) Xiang, H.; Xin, R.; Prasongthum, N.; Natewong, P.; Sooknoi, T.; Wang, J.; Reubroycharoen, P.; Fan, X. Catalytic Conversion of Bioethanol to Value-Added Chemicals and Fuels: A Review. *Resources Chemicals and Materials* **2022**, *1* (1), 47−68.

(29) Rossetti, I.; Tripodi, A.; Ramis, G. Hydrogen, Ethylene and Power Production from Bioethanol: Ready for the Renewable Market? *Int. J. Hydrogen Energy* **2020**, *45* (17), 10292−10303.

(30) Portarapillo, M.; Danzi, E.; Guida, G.; Luciani, G.; Marmo, L.; Sanchirico, R.; Di Benedetto, A. On the Flammable Behavior of Non-Traditional Dusts: Dimensionless Numbers Evaluation for Nylon 6,6 Short Fibers. *J. Loss Prev Process Ind.* **2022**, *78*, 104815.

(31) Aspen Technology. *Aspen Physical Property System - Physical Property Methods and Models 11.1* Aspen Technology, Inc.: Cambridge, MA 2001.

https://doi.org/10.1021/acsomega.3c07277
ACS Omega 2024, 9, 7793−7805

(32) Tsai, J.-C.; Lo, Y.-L.; Lin, C.-Y.; Sheu, H.; Lin, J.-C. Feasibility of Rapid Quantitation of Stratum Corneum Lipid Content by Fourier Transform Infrared Spectrometry. *J. Spectrosc.* **2004**, *18*, 423.
(33) Figen, A. K.; Pikin, S. Parametric Investigation on Anhydrous Sodium Metaborate (NaBO2) Synthesis from Concentrated Tincal. *Adv. Powder Technol.* **2010**, *21* (5), 513−520.
(34) Ma, Y.; Wang, J.; Zhang, Y. TG-FTIR Study on Pyrolysis of Enteromorpha Prolifera. *Biomass Convers Biorefin* **2018**, *8* (1), 151−157.
(35) Singh, R. K.; Ruj, B.; Sadhukhan, A. K.; Gupta, P. A TG-FTIR Investigation on the Co-Pyrolysis of the Waste HDPE, PP, PS and PET under High Heating Conditions. *Journal of the Energy Institute* **2020**, *93* (3), 1020−1035.
(36) Kumar, R.; Gunjal, J.; Chauhan, S. Effect of Borax-Boric Acid and Ammonium Polyphosphate on Flame Retardancy of Natural Fiber Polyethylene Composites. *Maderas: Ciencia y Tecnologia* **2022**, *24* (24), 1−10.
(37) Dogan, M.; Dogan, S. D.; Savas, L. A.; Ozcelik, G.; Tayfun, U. Flame Retardant Effect of Boron Compounds in Polymeric Materials. *Composites Part B* **2021**, *222*, 109088.
(38) Tsodikov, M. V.; Yandieva, F. A.; Kugel, V. Y.; Chistyakov, A. V.; Gekhman, A. E.; Moiseev, I. I. Reductive Dehydration of Ethanol: A New Route towards Alkanes. *Catal. Lett.* **2008**, *121* (3−4), 199−208.
(39) Ibrahim, N. A. Benzyl Alcohol. *Reference Module in Biomedical Sciences* **2023**, *2*, 17.
(40) Younes, M.; Aquilina, G.; Castle, L.; Engel, K. H.; Fowler, P.; Fürst, P.; Gürtler, R.; Gundert-Remy, U.; Husøy, T.; Mennes, W.; Moldeus, P.; Oskarsson, A.; Shah, R.; Waalkens-Berendsen, I.; Wölfle, D.; Boon, P.; Crebelli, R.; Di Domenico, A.; Filipič, M.; Mortensen, A.; Van Loveren, H.; Woutersen, R.; Gergelova, P.; Giarola, A.; Lodi, F.; Frutos Fernandez, M. J. Re-Evaluation of Benzyl Alcohol (E 1519) as Food Additive. *EFSA J.* **2019**, *17* (10), e05876.
(41) Rodrigues, C. J. C.; de Carvalho, C. C. C. R. Process Development for Benzyl Alcohol Production by Whole-Cell Biocatalysis in Stirred and Packed Bed Reactors. *Microorganisms* **2022**, *10* (5), 966.
(42) Wiedemann, T.; Voit, G.; Tchernook, A.; Roesle, P.; Göttker-Schnetmann, I.; Mecking, S. Monofunctional Hyperbranched Ethylene Oligomers. *J. Am. Chem. Soc.* **2014**, *136* (5), 2078−2085.
(43) Guo, L.; Liu, W.; Li, K.; Sun, M.; Sun, W.; Zhao, L.; Jiang, G.; Peng, H.; Liu, Z.; Dai, S. Synthesis of Functional and Hyperbranched Ethylene Oligomers Using Unsymmetrical α-Diimine Palladium Catalysts. *Eur. Polym. J.* **2019**, *115*, 185−192.
(44) Anil, S.; Indraja, S.; Singh, R.; Appari, S.; Roy, B. A Review on Ethanol Steam Reforming for Hydrogen Production over Ni/Al2O3 and Ni/CeO2 Based Catalyst Powders. *Int. J. Hydrogen Energy* **2022**, *47* (13), 8177−8213.
(45) Vicente, J.; Ereña, J.; Montero, C.; Azkoiti, M. J.; Bilbao, J.; Gayubo, A. G. Reaction Pathway for Ethanol Steam Reforming on a Ni/SiO2 Catalyst Including Coke Formation. *Int. J. Hydrogen Energy* **2014**, *39* (33), 18820−18834.
(46) Foucaud, Y.; Lainé, J.; Filippov, L. O.; Barrès, O.; Kim, W. J.; Filippova, I. V.; Pastore, M.; Lebègue, S.; Badawi, M. Adsorption Mechanisms of Fatty Acids on Fluorite Unraveled by Infrared Spectroscopy and First-Principles Calculations. *J. Colloid Interface Sci.* **2021**, *583*, 692−703.
(47) Ibrahim, M.; Nada, A.; Kamal, D. E. Density Functional Theory and FTIR Spectroscopic Study of Carboxyl Group. *Indian J. Pure Appl. Phys.* **2005**, *43*, 911−917.
(48) Kibar, M. E.; Akın, A. N. A Novel Process for CO2 Capture by Using Sodium Metaborate. Part I: Effects of Calcination. *Environmental Science and Pollution Research* **2018**, *25* (4), 3446−3457.

https://doi.org/10.1021/acsomega.3c07277
ACS Omega 2024, 9, 7793−7805